ISSN 1392–1320 MATERIALS SCIENCE (MEDŽIAGOTYRA). Vol. 28, No. 2. 2022

High Temperature Oxidation Resistance Performance of TiC/Mo Composite by Spark Plasma Sintering

Renheng HAN [1], Ziming BAO [1], Yanqin ZHU [1], Ning LI [1], Ming TANG [1], Hexin ZHANG [1, 2], Chengzhi ZHAO [1, 2] *

[1] *College of Materials Science and Chemical Engineering, Harbin Engineering University, No. 145 Nantong Avenue, Harbin, Heilongjiang, 150001, China*
[2] *Key Laboratory of Superlight Materials and Surface Technology of Ministry of Education, Harbin Engineering University, No. 145 Nantong Avenue, Harbin, Heilongjiang, 150001, China*

crossref http://dx.doi.org/10.5755/j02.ms.27486

Received 24 August 2020; accepted 05 January 2021

In this paper, the Titanium carbide/Molybdenum (TiC/Mo) alloy was prepared by spark plasma sintering (SPS). The oxidation process of the TiC/Mo alloy at different oxidation temperatures was studied, and the oxidation mechanism was discussed in depth. The focus is on the influence of the introduction of TiC particles on the high-temperature oxidation properties of Mo alloys. The phase composition and morphology of the oxide film were analyzed by means of X-ray diffraction (XRD), scanning electron microscopy (SEM), and energy dispersive spectroscopy (EDS). The results showed that, after oxidation, the surface oxide film is mainly composed of Titanium dioxide (TiO_2), Molybdenum dioxide (MoO_2), Molybdenum trioxide (MoO_3) and Molybdenum oxide hydrate ($MoO_3(H_2O)_2$) phases. As the oxidation temperature increases, the surface of the oxide film will warp, and thereby increase porosity. The dense MoO_2 will form a protective inner oxide layer and inhibit further progress of the TiC/Mo alloy. Oxygen will undergo violent oxidation through the pores and the inside of the matrix, and the protective MoO_2 internal oxide film will disappear. TiC particles dispersed in the matrix will be oxidized to form TiO_2, which will be gradually deposited on the surface of the oxide film, hindering the diffusion of oxygen to the matrix. The quantity loss during the entire oxidation process is significantly reduced. Therefore, the introduction of TiC can greatly improve the oxidation resistance of Mo alloys.
Keywords: heat-temperature oxidation, composite materials, TiC, Mo alloy.

1. INTRODUCTION

Owing to its high melting point and excellent high temperature performance, molybdenum and its alloys have higher operating temperatures than iron and nickel-based superalloys, and are widely used in cutting-edge fields such as the nuclear industry and aerospace [1, 2]. With the continuous development of science and technology, stricter requirements are being introduced for high-temperature materials [3]. Considering that the traditional sintering process requires a lot of time and high sintering temperature, it is very likely to obtain a structure with coarse grains, and this could affect the overall performance of a material [4, 5]. In recent years, the spark plasma sintering method has gained popularity as an effective nonconventional sintering technique. The ions generated by the high-frequency pulse current have the effect of activating and cleaning the surface of particles, effectively reducing the sintering temperature and time. For this reason, this method has attracted the attention of various scientific research institutions [6, 7]. The spark plasma sintering method has the advantage of significantly short production cycles and sintering times, and is an effective means of obtaining high-density, fine-grained molybdenum materials [8].

Although molybdenum and molybdenum alloys have high melting points, good high-temperature mechanical properties, and lower density, they are easily oxidized at high temperatures [9]. Molybdenum starts to oxidize significantly at 400 ℃, thereby generating volatile MoO_3, and this greatly limits its application in high temperature fields [10]. At present, there are two main ways of improving the oxidation resistance of molybdenum alloys [11]. One is to make the molybdenum alloy matrix achieve self-oxidation resistance through alloying, and the other is to coat the surface of the molybdenum alloy with an oxidation-resistant coating [12]. Although the protective coating provides excellent oxidation resistance, it is greatly affected by thermal matching and thermal shock during the preparation process; also, the coating process may affect the structure and mechanical properties of the molybdenum alloy [13]. Most researchers on the use of alloying to improve the oxidation resistance of molybdenum alloys focus on Mo-Si-B alloy systems [14]. The T2 phase (Mo_5SiB_2) of the alloy matrix can form a layer that inhibits oxidation, and this ensures the alloy has excellent oxidation resistance. However, the brittleness of the Mo-Si-B alloy severely limits its application in structural materials [15]. How to harmonize the relationship between mechanical properties and oxidation resistance has become an urgent matter. TiC has the attributes of high hardness, high wear resistance and excellent high temperature oxidation

* Corresponding author. Tel.: +86-13895718408.
E-mail address: *zhaochengzhi@hrbeu.edu.cn* (C. Zhao)

resistance [16]. Compared with molybdenum, it has better affinity for oxygen and forms a protective oxide film more easily, thereby improving the oxidation resistance of a material [17]. Therefore, it is necessary to study in detail the effect of introducing TiC on the high temperature oxidation properties of Mo alloy.

In this study, the molybdenum matrix was solid-solution strengthened and dispersion strengthened by adding TiC. The oxidation kinetic curve was then derived. Further, the oxidation morphology, energy spectrum and phase analysis of the TiC/Mo alloy at different temperatures and oxidation times were analyzed. This study is an in-depth exploration of the alloy's oxidation mechanism, and lays a foundation for further research on molybdenum alloys.

2. MATERIALS AND METHODS

2.1. Materials

The SPS equipment used in this experiment is the LHPD250 equipment designed and manufactured by FCT. The test components comprised Mo-5 wt.% TiC (hereafter collectively referred to as TiC/Mo alloy). The element powders are mixed via the ball mill process. The parameters of the ball mill are as follows: the ball-to-material ratio is 2:1, the ball milling time is 5 h, and the rotation speed is 200/rpm. The ball mill tank is filled with argon as a protective gas. The ball mill process is as follows: after dry mixing, the powder is compacted at the bottom of the ball mill tank, and then the ball floats on it. Then, ethanol is added as the ball milling medium and the mixing is continued. The powder is then treated in a vacuum drying oven at 100 °C for 1 hour, and then sieved through a 200 mesh sieve. Then, an analytical balance is used to measure 300 grams of powder, which is placed inside a Ø 40 graphite mold. Before charging, the graphite paper is first attached to the inside of the mold and the contact surface between the head and the powder. Then, the mold is placed in the SPS furnace. The temperature is set to rise from room temperature to 1700 °C at a rate of 100 K/min, and the pressure is set to rise from 5 MPa to 30 MPa. Then, this temperature is maintained for 9 minutes, and the contents are finally cooled in a furnace.

2.2. Methods

In this experiment, the SM-28-10 high-temperature resistance furnace was used to perform the high-temperature oxidation test. The TiC/Mo alloy sample was cut into rectangular blocks with a size of 10 mm × 20 mm × 1.5 mm. After grinding and polishing, the sample was ultrasonically cleaned with ethanol and dried for use. Based on the cyclic oxidation test method, the samples were subjected to high temperature oxidation at 400 °C, 600 °C, 800 °C and 1000 °C. The oxidation times are 5 minutes, 10 minutes, 20 minutes, 30 minutes and 60 minutes. An analytical balance with an accuracy of 0.0001 g was used to measure the mass change before and after oxidation.

Further, before analysis, a non-conductive oxide was deposited on the sample (3ΔL-TEC type SCD005). The phase analysis of the material was performed using X-ray diffraction (XRD) (X Pert Pro) at CuKα radiation (λ = 1.5406Å) and 2θ in the range of 10° to 90°. Microstructure observation and composition analysis were performed using a scanning electron microscope (SEM) and energy dispersive spectroscopy (EDS) (Quanta 200, FEI Company). The voltage of the scanning electron microscope is 15 kV.

3. RESULTS AND DISCUSSION

3.1. The oxidation kinetic curve of the TiC/Mo alloy

Fig. 1 shows the mass loss rate curve of the TiC/Mo alloy and pure Mo content oxidized at 1000 ℃. It can be seen that as the oxidation time increases, the mass loss rate of both the TiC/Mo alloy and pure Mo gradually increases.

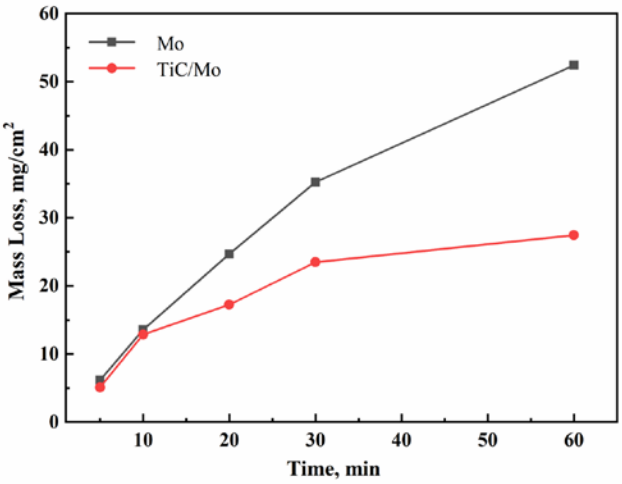

Fig. 1. The oxidation kinetic curve of the TiC/Mo alloy and Mo at 1000 ℃

When the oxidation time reaches 60 min, the mass loss rate of pure Mo is 53.43 %, while the mass loss rate of the TiC/Mo alloy is 26.91 %. This means the oxidation kinetic curves of the two alloys conform to the parabolic law. After the initial oxidation time of 10 minutes, there is no much difference in the mass loss of the two alloys. A more obvious phenomenon is that with the increase of oxidation time, the quantity loss of the TiC/Mo alloy is much smaller than that of pure Mo. The difference in mass loss rate between the TiC/Mo alloy and pure Mo shows an increasing trend, and is related to the Mo content [18]. As the oxidation progresses, the Mo element is oxidized to produce volatile MoO_3, and the pores formed on the substrate increase. However, the more pores are formed in the oxidation process of Mo, the easier it is for the material to be corroded by oxygen, and this could greatly increase the mass loss rate. The results of oxidation experiments show that the introduction of TiC can effectively prevent the corrosion of the TiC/Mo alloy by oxygen.

3.2. XRD phase analysis of the TiC/Mo alloy

Fig. 2 presents the XRD spectrum of the oxide layer of the TiC/Mo composite material after 60 minutes of oxidation at different temperatures. It can be seen that the surface of the substrate is mainly composed of Mo and Mo_2C when oxidized at 400 °C, and that small amounts of the MoO_3 phase and the monoclinic dihydrate $(MoO_3(H_2O)_2)$ are formed.

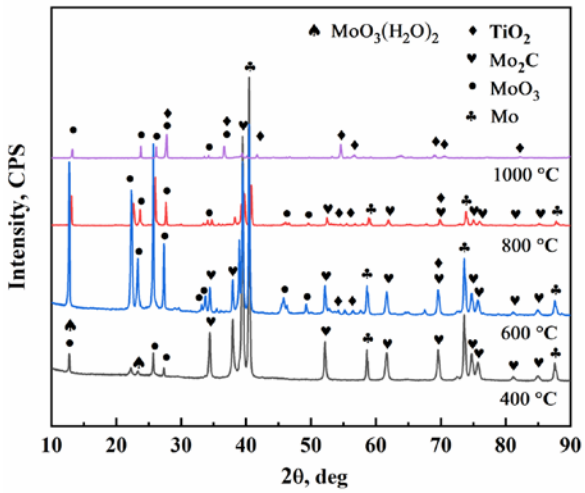

Fig. 2. XRD spectra of the oxide layer of the TiC/Mo composite at different oxidation temperatures

When the temperature rises to 600 ℃, a large amount of the MoO_3 phase is formed. Although $MoO_3(H_2O)_2$ disappears, both Mo and Mo_2C can still be detected on the surface. The peak height of the XRD spectrum can approximately reflect the content of the phase [19]. With increasing temperature, the peak values of both Mo and Mo_2C decrease significantly, and when the temperature reaches 800 ℃, a small amount of TiO_2 begins to appear. When the temperature is 1000 ℃, a large amount of TiO_2 is formed on the oxidized surface, which mainly contains the two phases of MoO_3 and TiO_2.

3.3. SEM surface morphology of the TiC/Mo alloy after oxidation at different temperatures

Fig. 3 presents a photomicrograph of the oxidized surface morphology of the TiC/Mo composite material at temperatures of 400 ℃, 600 ℃, 800 ℃ and 1000 ℃ over the duration of 60 minutes.

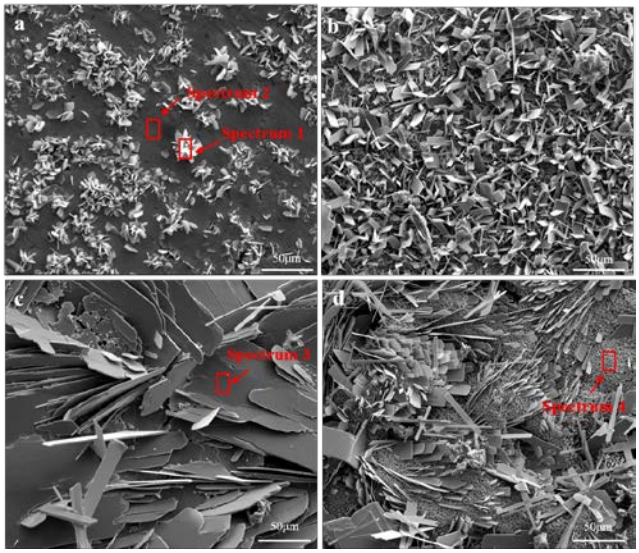

Fig. 3. Micrographs of the oxidized surface morphology of the TiC/Mo composite after oxidation at different temperatures. Surface morphology of the sample TiC/Mo composites oxide film at: a – 400 °C; b – 600 °C; c – 800 °C; d – 1000 °C

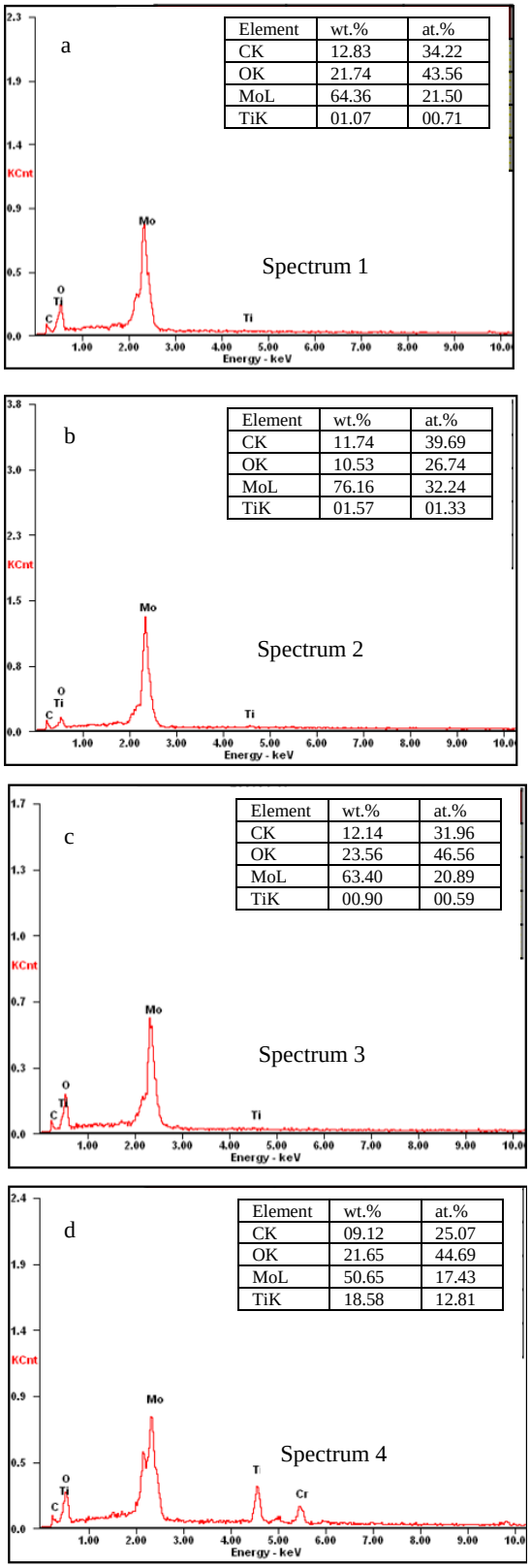

Fig. 4. EDS analysis of the oxidized surface morphology of the TiC/Mo composite material shown in Fig. 3 at different oxidation temperatures. Spectrum 1, 2, 3 and 4 of the surface morphology of the sample TiC/Mo composites oxide film shown in Fig. 3: a – 400 °C; b – 600 °C; c – 800 °C; d – 1000 °C

As shown in Fig. 3, as the oxidation temperature increases, the warpage of the oxide film surface becomes

more and more apparent. The oxide film is generally divided into granular and flaky tissues, and the average size of the granular tissue is less than 1 μm. Based on the XRD analysis of previous related literature [20], the particulate matter is mainly TiO_2 and the flaky structure is mainly MoO_3. When the oxidation temperature is 400 °C, the surface of the oxide film is mainly composed of small white fragments, which are either inlaid or protruding from the surface of the substrate. When the oxidation temperature is 600 °C, a large number of small-sized flaky tissue matrix appears on the surface of the oxide film. Meanwhile, the reaction between the matrix and oxygen is obviously intensified, and the loosely arranged products almost cover the entire metal surface. At this time, no obvious TiC particles are observed on the surface. As the oxidation temperature increases, the flaky structure thickens and evaporates. When the oxidation temperature reaches 1000 °C, the large-sized flakes on the surface evaporate quickly, and a granular structure is continuously deposited, forming a morphology in which the granular structure and the flake structure coexist. The deposited granular TiO_2 gradually covers the surface of the oxide film, thereby preventing oxygen from penetrating further into the substrate and effectively inhibiting the oxidation process.

The EDS analysis of the calibrated microzone shown in Fig. 3 is presented in Fig. 4. Fig. 4 a and c present the results of the energy spectrum analysis of microzones 1 and 3 in Fig. 3, and the main area is the flaky structure on the surface of the oxide film. The symbol *CK* represents the characteristic peak produced by the carbon element in the K-line system during the test, and the symbol *MoL* represents the characteristic peak produced by the molybdenum element in the L-line system during the test. The symbols *OK* and *TiK* represent the same principles as above. According to the results of energy spectrum analysis and XRD analysis, the fragmented oxidation products are mainly MoO_3. As shown in Fig. 3 a and Fig. 4 b, the energy spectrum analysis of the dark gray spectrum 2 indicates that oxygen in this region is significantly reduced, and that Mo and Ti elements have increased.

This is because of the presence of unreacted Mo, Mo_2C matrix and TiC particles in this region. When the oxidation temperature is low, the oxidation reaction is weak. Additionally, part of the matrix does not fully react with oxygen, and even though oxygen can be detected, there is no obvious shape difference. When the temperature reaches 1000 °C, the surface is largely composed of flake MoO_3 and many small particles, which are interspersed by the MoO_3. The results of energy spectrum analysis of the particulate matter in spectrum 4 are presented in Fig. 4 d. The energy spectrum shows that the content of the Ti element has increased greatly, and the morphology shows the presence of TiO_2 particles.

3.4. SEM cross-section morphology analysis of the TiC/Mo alloy after oxidation at different temperatures

Fig. 5 shows the oxidation cross-section morphology and line scan energy spectrum of the oxide layer of the TiC/Mo alloy at different oxidation temperatures.

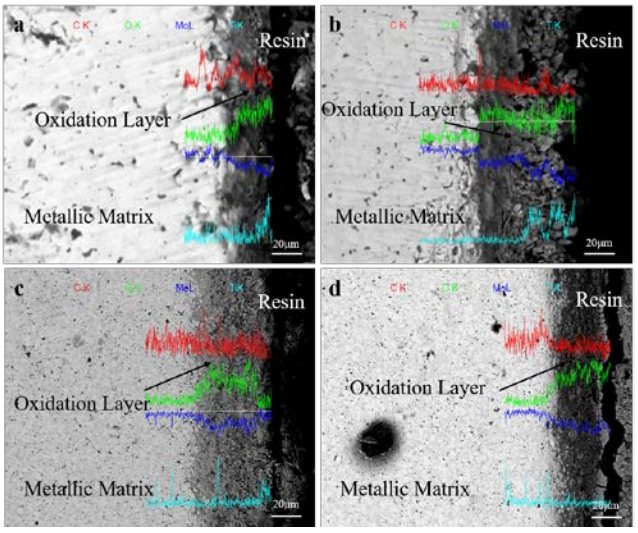

Fig. 5. Oxidation cross-section morphology and EDS line scan energy spectrum of the oxide layer of the TiC/Mo alloy at different oxidation temperatures. Cross-section morphology of the sample TiC/Mo composites oxide film at: a – 400 °C; b – 600 °C; c – 800 °C; d – 1000 °C

It can be clearly seen from Fig. 5 that as the oxidation temperature increases, there is a corresponding increase in the thickness of the oxide layer. According to previous related literature [21], the introduction of TiC reduces the oxidation degree of the Mo alloy and improves the oxidation resistance of the TiC/Mo alloy. This is mainly because TiC has a higher affinity for oxygen in the atmosphere than Mo, and this makes it easier to form TiO_2, which subsequently reduces the rate of formation of MoO_3 as well as the porosity of the cross section. As a result, the oxidation resistance of the alloy is improved. In general, a transition layer that consists of a low-quality oxide forms under the surface of the MoO_3, and the composition of this layer is MoO_x ($2 < x < 3$) [22]. MoO_2, as an intermediate product of oxidation, has the ability to form a relatively dense internal oxide film in the oxide layer. It can be seen from Fig. 5 that this phenomenon is obvious when the oxidation temperature is 600 °C and 800 °C. When the temperature is low, the content of MoO_3 is less and the surface warpage is not obvious, and it is not easy for the oxide film to achieve delamination. When the temperature is higher, the internal MoO_2 is fully oxidized and the internal oxide layer disappears. According to analysis of the elements in the EDS line scan, the content of Mo in the oxide layer is significantly lower than that in the matrix. It is clear that the Ti element content increased slightly, the O element content increased significantly, and the C element content decreased significantly. Obviously, this also confirms that TiC fully reacted with O_2 in the oxide layer.

3.5. Discussion

Fig. 6 is a schematic diagram of the oxidation process of the TiC/Mo alloys at different oxidation times. As the alloy sample is heated with the furnace at room temperature, as the heating time increases, the temperature of the alloy surface also rises correspondingly. It can be clearly seen from Fig. 6 a that after the TiC/Mo alloy is sintered, the

metal matrix is largely composed of Mo, and that TiC has been partially dispersed in Mo_2C in the matrix [23].

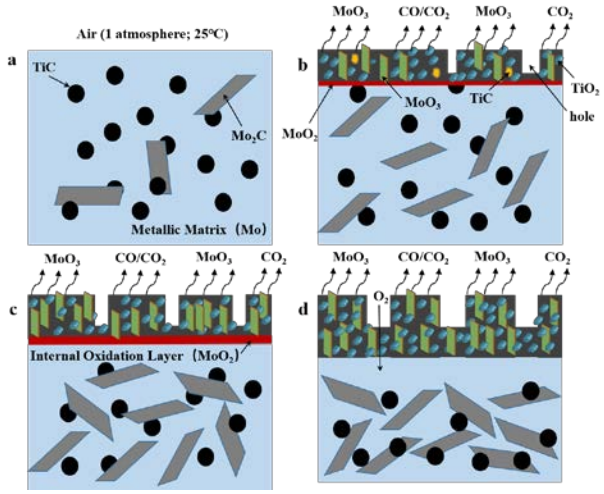

Fig. 6. Schematic diagram of the oxidation process of the TiC/Mo alloy at different oxidation temperatures. Cross-section morphology of the sample TiC/Mo composites oxide at: a – 0 min; b – 10 min; c – 30 min; d – 60 min

The oxidation resistance of the material is closely related to the compactness of the material itself and the oxidation characteristics of the generated oxide. Analyzing the reaction of materials in the oxidation process is of great significance for understanding their oxidation mechanism and improving their oxidation resistance. When the TiC/Mo alloy system is oxidized at high temperature, the following reactions occur [24]:

The matrix Mo and Mo_2C produced during the sintering process react with O_2 to form MoO_2 and MoO_3, as shown in Eq. 1 – Eq. 4:

$$Mo + O_2 \rightarrow MoO_2; \quad (1)$$

$$2MoO_2 + O_2 \rightarrow 2MoO_3; \quad (2)$$

$$2Mo + 3O_2 \rightarrow 2MoO_3; \quad (3)$$

$$Mo_2C + 4O_2 \rightarrow 2MoO_3 + CO_2. \quad (4)$$

The dispersed TiC in the Mo matrix reacts with O_2 to form TiO_2, as shown in Eq. 5:

$$TiC + 2O_2 \rightarrow TiO_2 + CO_2. \quad (5)$$

Molybdenum alloys are more prone to oxidation at high temperatures, and they begin to oxidize when heated to about 300 °C in air atmosphere. In the initial stage of oxidation, the TiC/Mo alloy will form a dense adhesive oxide film, and a cyan oxide film will cover the surface. The oxidation rate of the oxide film depends on the diffusion rate of metal ions (M^{n+}) and oxygen through the oxide film. At this stage, the oxidation is relatively slow, and the growth rate of the oxide film is low. With the continuous increase of the oxidation temperature, the inner oxide layer of MoO_2 reaches a certain thickness, and the volatilization of MoO_3 occurs while the oxide film is being formed. This is because, at this time, MoO_2 is oxidized to form MoO_3, whose formation rate is equal to its volatilization rate, which increases with the increase of oxidation temperature and pressure [25]. It can be seen from Fig. 6 b that as the oxidation time increases, a large amount of dark green gas starts to rise from the surface of the sample. This is because the MoO_3 gas generated by the oxidation of Mo and Mo_2C forms a dark green oxide on the surface of the oxide film. Additionally, the surface of the oxide layer begins to warp, and porosity increases gradually. The MoO_3 and CO_2 gases in Fig. 6 b are the reaction products of Mo, Mo_2C and TiC.

When the oxidation time reaches 10 min, the surface of the oxidized sample is largely composed of granular and flaky structures. Combining XRD results and theoretical concepts [26], it can be known that the granular form is the TiO_2 phase, and the flake form is the MoO_3 phase. With the increase of the oxidation temperature, the warpage of MoO_3 becomes more apparent, and pores begin to appear on the surface of the oxide film of the TiC/Mo alloy. Oxygen erosion speeds up, and a large amount of Mo and Mo_2C in the matrix are exposed to the air, thereby reacting with oxygen. As the oxidation progresses violently and a large amount of MoO_2 and MoO_3 are generated, the thickness of the oxide film begins to increase rapidly. Relevant studies have shown that the structure of the oxide film at 600 °C will have obvious delamination, and that the inner layer is mainly MoO_2 and the outer layer is mainly MoO_3 [27]. As shown in Fig.6c, as the oxidation temperature increases, the inner oxide layer gradually thickens. The dense inner oxide layer inhibits the continued thickening of the oxide film. During this period, the under-oxidized MoO_2 mesophase and TiC particles in the outer oxide layer will continue to be oxidized into MoO_3 and TiO_2. The surface warpage of the oxide film will become more obvious, and the porosity will be further improved. Additionally, as shown in Fig. 6 d, when the inner oxide layer reaches critical thickness, cracking occurs causing the oxidation rate to accelerate sharply. Studies have shown that after the internal oxide layer ruptures at high temperatures, the oxidation rate is so fast that the heat released by the oxidation reaction does not manage to volatilize, and this produces an autocatalytic effect that makes the oxide film to increase abruptly [28].

Clearly, the introduction of TiC particles plays a very important role in reducing the oxidation resistance of Mo alloys. Compared with molybdenum, metallic titanium has a stronger affinity for oxygen. During oxidation, the TiC/Mo alloy reacts with oxygen to generate MoO_3 and TiO_2. MoO_3 volatilizes at high temperature, while TiO_2 is gradually deposited on the surface of the oxide film to form a protective oxide layer, which hinders the diffusion of oxygen to the substrate, thereby improving the high temperature oxidation resistance of the material [29]. In the initial stage of oxidation, the TiC/Mo alloy firstly undergoes oxidation reactions on areas with defects (such as pores, cracks, etc.) as well as grain boundaries on the surface of the substrate. After the easily oxidized molybdenum volatilizes after the formation of MoO_3, larger defects will be formed at defects on the substrate. This allows oxygen to further attack the matrix. However, the TiO_2 generated after TiC oxidation prevents oxygen from corroding the substrate. With the continuous deposition of TiC, the TiO_2 particles generated after oxidation are gradually densely connected together, inhibiting further erosion by oxygen. As oxidation progresses, TiO_2 particles are stacked on the surface of the substrate to form a granular structure that hinders the diffusion of oxygen ions from the outside to the inside. The oxidation rate is dictated by the diffusion speed of oxygen

through the oxide film, which effectively prevents diffusion of oxygen into the substrate, thereby hindering the erosion of the ceramic matrix by oxygen [30]. This is also consistent with the oxidation kinetic curve derived in previous studies.

4. CONCLUSIONS

In this study, the composition of the traditional molybdenum alloy is improved, and the ball-milled TiC/Mo mixed powder is prepared through rapid sintering by the spark plasma sintering method. The focus is on the influence of the introduction of TiC particles on the oxidation properties of Mo alloys. The following conclusions are obtained: as the oxidation temperature of the TiC/Mo composite material increases, the fragmented MoO_3 and denser MoO_2 are gradually formed on the surface of the oxide film. As the oxidation temperature increases further, the oxide film delaminates, and the inner layer is mainly MoO_2 and it has protective properties. This layer ruptures as the oxidation temperature increases, causing the oxidation rate to increase sharply. The fragmented MoO_3 in the outer layer increases in volume, becomes flaky in shape, and evaporates in large amounts. Titanium has a higher affinity for oxygen than molybdenum. The TiO_2 generated during the oxidation of TiC gradually deposits on the surface of the oxide film along with the volatilization of MoO_3 at high temperature, forming a protective oxide layer, which hinders the diffusion of oxygen to the substrate. Notably, the quantity loss of the entire oxidation process is significantly reduced, and the oxidation resistance of the TiC/Mo alloy is improved.

Acknowledgments

This research was Supported by Key Laboratory fund general projects (No. 6142905180203).

REFERENCES

1. **Sharna, I.G., Chakraborty, S.P., Suri, A.K.** Preparation of TZM Alloy by Aluminothermic Smelting and its Characterization *Journal of Alloys & Compounds* 393 (1) 2004: pp. 122 – 127. https://doi.org/10.1016/j.jallcom.2004.09.055
2. **Wang, Y., Wang, D., Yan, J., Sun, A.** Preparation and Characterization of Molybdenum Disilicide Coating on Molybdenum Substrate by Air Plasma Spraying *Applied Surface Science* 284 (1) 2013: pp. 881 – 888. https://doi.org/10.1016/j.apsusc.2013.08.029.
3. **Kong, G., Du, X., Cai. X., Feng, P.** Recycling Molybdenum Oxides from Waste Molybdenum Disilicides: Oxidation Experimental Study and Photocatalytic Properties *Oxidation of Metals* 92 (1 – 2) 2019: pp. 1 –12. https://doi.org/10.1007/s11085-019-09909-x
4. **Hachisuka, T., Nishimura, T., Kondo, M.** The Effect of Molybdenum on The Oxidation of TiC-Ni-Mo Alloys *Journal of the Japan Institute of Metals* 30 (3) 1966: pp. 296 – 301. https://doi.org/10.2320/jinstmet1952.30.3_296
5. **Jiang, Q.C., Fang, J.R., Guan, Q.F.** Oxidation and Volatilization of TZM Alloy In Air *Journal of Nuclear Materials* 283 (1) 2000: pp.1458 – 1462. https://doi.org/10.1016/S0022-3115(00)00303-2
6. **Zhu, Q., Shobu, K., Zeng, Y., Watanabe, T.** Oxidation Behavior of Hot-pressed $MoSi_2$-TiC Composite *Journal of Materials Science* 36 (2) 2001: pp. 313 – 319. https://doi.org/10.1023/A:1004851823360
7. **Zhu, Y.T., Shu, L., Butt, D.P.** Kinetics and Products of Molybdenum Disilicide Powder Oxidation *Journal of the American Ceramic Society* 85 (2) 2010: pp. 507 – 509. https://doi.org/10.1111/j.1151-2916.2002.tb00124.x
8. **Dzodziev, G.T., Shlyuko, V.Y., Palekha, K.K., Kantor, R.V.** Oxidizability of Materials Based on TiC and TiN at Elevated Temperatures *Soviet Powder Metallurgy & Metal Ceramics* 27 (4) 1988: pp. 323 – 325. https://doi.org/10.1007/BF00794456
9. **Wiedemeier, H., Singh, M.** Thermochemical Modelling of Interfacial Reactions in Molybdenum Disilicide Matrix Composites *Journal of Materials Science* 27(11) 1992: pp. 2974 – 2978. https://doi.org/10.1007/BF01154108
10. **Liu, N., Xu, Y., Li, Z., Chen, M., Li, G., Zhang, L.** Influence of Molybdenum Addition on the Microstructure and Mechanical Properties of TiC-based Cermets with Nano-TiN Modification *Ceramics International* 29(8) 2003: pp. 919 – 925. https://doi.org/10.1016/S0272-8842(03)00046-4
11. **Kitsunai, Y., Kurishita, H., Kuwabara, T., Narui, M., Hasegawa, M., Takida, T.** Radiation Embrittlement Behavior of Fine-grained Molybdenum Alloy with 0.2 wt% TiC Addition *Journal of Nuclear Materials* 346 (2-3) 2005: pp. 233 – 243. https://doi.org/10.1016/j.jnucmat.2005.06.013
12. **Yang, G., Liu, Z., Wang, Y.** Influence of Molybdenum on the Microstructure and Mechanical Properties of TiC-TiB_2 Reinforced Metal Matrix Composite Coatings *Science China Technological Sciences* 04 2013: pp. 1008 – 1016. https://doi.org/10.1007/s11431-013-5150-4
13. **Schneibel, J.H., Tortorelli, P.F., Ritchie, R.O., Kruzic, J.J.** Optimization of Mo-Si-B Intermetallic Alloys *Metallurgical & Materials Transactions A* 36 (3) 2005: pp. 525 – 531. https://doi.org/10.1007/s11661-005-0166-4
14. **Ervin, D.R., Bourell, D.L., Persad, C., Rabenberg, L.** Structure and Properties of High Energy, High Rate Consolidated Molybdenum Alloy TZM *Materials Science & Engineering A* 102 (1) 1988: pp. 25 – 30. https://doi.org/10.1016/0025-5416(88)90529-0
15. **Guo, Z., Xiong, J., Yang, M., Song, X., Jiang, C.** Effect of Mo_2C on the Microstructure and Properties of WC-TiC-Ni cemented carbide *International Journal of Refractory Metals & Hard Materials* 26(6) 2008: pp. 601 – 605. https://doi.org/10.1016/j.ijrmhm.2008.01.007
16. **Wang, J., Li, W.Z., Li, H.D.** Preparation and Characterization of Superhard TiC/Mo Multilayers *Journal of Materials Science* 35 (11) 2000: pp. 2689 – 2693. https://doi.org/10.1023/A:1004797724460
17. **Yuping, Z., Xu, C.N., Watanabe, T.** The Effects of Carbon Addition on the Mechanical Properties of $MoSi_2$-TiC Composites *Ceramics International* 28 (4) 2002: pp. 387 – 392. https://doi.org/10.1016/S0272-8842(01)00106-7
18. **Zhang, J., Pan, C., Fang, P., Wei, J., Xiong, R.** Mo+C Codoped TiO(2) Using Thermal Oxidation for Enhancing Photocatalytic Activity *ACS Applied Materials and Interfaces* 2 (4) 2010: pp. 1173 – 1176. https://doi.org/10.1021/am100011c

19. **Xu, L., Yang, Y., Wang, S., Li, M., Xu, J., Qian, Y.** Improved Both Mechanical and Anti-oxidation Performances of ZrB_2-SiC Ceramics with Molybdenum Disilicide Addition *Materials Chemistry & Physics* 223 2019: pp. 53 – 59. https://doi.org/10.1016/j.matchemphys.2018.10.044
20. **Zhou, W., Sun, X., Kikuchi, K., Nomura, N., Yoshimi, K., Kawasaki, A.** In Situ Synthesized TiC/Mo-based Composites Via Laser Powder Bed Fusion *Materials & Design* 146 2018: pp. 116 – 124. https://doi.org/10.11901/1005.3093.2015.230
21. **Leonard, K.J., Busby, J.T., Zinkle, S.J.** Aging Effects on Microstructural and Mechanical Properties of Select Refractory Metal Alloys for Space-reactor Applications *Journal of Nuclear Materials* 366 (9) 2007: pp. 336 – 352. https://doi.org/10.1016/j.jnucmat.2007.03.025
22. **Lan, S., Sheng, P.J.** Mechanical Properties of TiC Particles Reinforced MoSi-2 Composites *Journal of Materials Engineering* 53 (6S) 2001: pp. 31 – 34. https://doi.org/10.7567/JJAP.53.06JG14
23. **Cédat, D., Fandeur, O., Rey, C., Raabe, D.** Polycrystal Model of the Mechanical Behavior of a Mo-TiC 30vol.% Metal-Ceramic Composite Using a Three-dimensional Microstructure Map Obtained by Dual Beam Focused Ion Beam Scanning Electron Microscopy *Acta Materialia* 60 (4) 2012: pp. 1623 – 1632. https://doi.org/10.1016/j.actamat.2011.11.055
24. **Rosner, D.E., Allendorf, H.D.** Kinetics of High-Temperature Oxidation of Molybdenum by Dissociated Oxygen *Vacuum* 40 (11) 1964: pp. 3441 – 3442. https://doi.org/10.1063/1.1725022
25. **Chang, Y.A.** Oxidation of Molybdenum Disilicide *Journal of Materials Science* 4 (7) 1969: pp. 641 – 643. https://doi.org/10.1007/BF00550120
26. **Tomasi, A., Ceccato, R., Nazmy, M., Gialanella, S.** Microstructure and Oxidation Behaviour of Chromium-Molybdenum Silicides *Materials Science & Engineering A* 240 (1) 1998: pp. 877 – 881. https://doi.org/10.1016/S0921-5093(97)00678-3
27. **Magnani, G., Brentari, A., Burresi, E., Coglitore, A.** Mechanical Properties and Oxidation Behavior of Silicon Carbide-molybdenum Silicides Composites *Ceramics International* 39 (3) 2013: pp. 3445. https://doi.org/10.1016/j.ceramint.2012.10.024
28. **Ohser-Wiedemann, R., Weck, C., Martin, U.** Spark Plasma Sintering of TiC Particle-reinforced Molybdenum Composites *International Journal of Refractory Metals & Hard Materials* 32 (5) 2011: pp. 1 – 6. https://doi.org/10.1016/j.ijrmhm.2011.12.001
29. **Kim, G.S., Hai, G.K., Kim, D.G.** Densification Behavior of Mo Nanopowders Prepared by Mechanochemical Processing *Journal of Alloys & Compounds* 469 (1) 2009: pp. 401 – 405. https://doi.org/10.1016/j.jallcom.2008.01.149
30. **Li, B., Wang, J., Chen, X., Lin, X., Zhang, G.** High-temperature Oxidation Response of Mo-Si-B Composites with TiO_{2w}/SiC_w Addition *Ceramics International* 45 (13) 2019: pp. 3441 – 3442. https://doi.org/10.1016/j.ceramint.2019.05.120

© Han et al. *2022* Open Access This article is distributed under the terms of the Creative Commons Attribution 4.0 International License (http://creativecommons.org/licenses/by/4.0/), which permits unrestricted use, distribution, and reproduction in any medium, provided you give appropriate credit to the original author(s) and the source, provide a link to the Creative Commons license, and indicate if changes were made.